Modelling and Control of a Turbocharged Burner Unit

Brian Solberg[1], Palle Andersen[2] and Jakob Stoustrup[2]

[1]Aalborg Industries A/S, Aalborg, Denmark, bso@es.aau.dk
[2]Aalborg University, Aalborg, Denmark, {pa,jakob}@es.aau.dk

ABSTRACT: This paper concerns modelling and control of a novel turbocharged burner unit developed for small-scale industrial and marine boilers. The burner consists of a gas turbine mounted on a furnace. The burner has two inputs; oil flow to the gas generator (gas turbine combustion chamber) and oil flow to the furnace, and two outputs; power and oxygen percentage in the exhaust gas. The control objective of the burner unit is to deliver the requested power set by e.g. an outer pressure loop while keeping a clean combustion and optimising efficiency. A first principle model is derived and validated against preliminary test data. The preliminary test shows that the model is capable of capturing the important dynamics of the burner unit while more testing is required to determine the reason for discrepancies in gains. An analysis of the model shows that both dynamics and gains change remarkably over the entire load range. However, local linearised models of low order can be derived and used in a subsequent controller design. Also, the model includes an inverse response (non-minimum phase zero) from the gas generator oil flow to the controlled oxygen level. This means that when changing the oil flow to the gas generator, the oxygen level initially moves in the opposite direction before it moves in the long term direction. A control strategy based on a nonlinear feedforward and a linear feedback controller, adjusting the ratio between the oil flow to the gas generator and to the furnace, is proposed. The feedforward is calculated from an inverse mapping of the requested power output to find the two stationary oil flows while respecting oxygen constraints. Simulation results gathered from the developed nonlinear model with added noise and external disturbances illustrate the efficiency of the proposed control strategy.

Keywords: turbocharger, gas turbine, first principle modelling, lumped parameter models, burner control

1 INTRODUCTION

Most burners, shipped with industrial and marine boilers today, are equipped with a fan to supply the combustion with air. Such fans consume considerable amounts of electric power and produce noise. Further, to achieve a high turndown ratio using a conventional burner, more than one atomiser is needed. The burner considered in this paper is a two stage burner in which the first stage drives a gas turbine and the second stage is a conventional furnace burner. This concept has multiple advantages over the aforementioned fan concept. First of all burner efficiency is high as there is no longer a need for electrical fan actuation. Further, the turndown ratio is increased in the way that the gas turbine can operate alone (however, this operation mode is not very thermodynamically efficient). Finally, the gas turbine concept increases the gas ve-

locity through the boiler convection part which leads to a higher heat transfer to the metal.

However, this new burner concept requires a more comprehensive control strategy than the conventional burners to maximise efficiency and keep a clean combustion to e.g. minimise the amount of pollutant expelled from the funnel. This factor is especially important when the burner is installed on ship boilers as large penalties are assigned to shipowners if the smoke coming out of the stacks is too harmful to the environment.

The control problem is complicated by the high degree of nonlinearities in the system and further, the process exhibits an inverse response from the gas generator (gas turbine combustion chamber) fuel injection to the flue gas oxygen level which is used as a parameter for clean combustion.

In relation to the automotive industry many people have addressed modelling and control of turbocharged diesel engines – see e.g. [1, 2, 3, 4]. From these works, results on the turbocharger modelling can be used. There is obviously a resemblance between the setup presented in this paper and the gas turbine found on power plants and combined cycle power plants. A model of a stationary gas turbine can be found in [5].

We derive a model based on first principles rather than using system identification techniques to specify a black box model based on e.g. linear parametric models. This technique is adopted as these models tend to be valid over a wider operating range. The goal is to derive a lumped parameter model that reflects the burner dynamics as well as possible from knowledge of the system behaviour and measurement. This approach is also taken to achieve insight to the burner process. Further, a detailed model like this will be of great value as a simulation platform for controller designs. Model verification experiments have been performed at Aalborg Industries' (AI) test centre.

Regarding controller design, principles such as traditional selector and ratio control of burners can be used – see e.g. [6]. However, many other methods exist and especially model predictive control (MPC) [7, 8, 9] is an interesting candidate as it can naturally handle constraints on inputs and state variables. However, in this paper we focus on the control properties of the burner unit and therefore stick with traditional selector and ratio control with a nonlinear feedforward from setpoint changes.

We show that even though the process is nonlinear and includes inverse responses, a simple ratio controller can control the process. However, if more advanced control methods are to be used it is expected to be necessary to handle the nonlinearities in the control setup.

The paper is organised as follows: First a short system description is given and assumptions made for modelling purposes are presented. Leading is the model derivation followed by a discussion of the control properties. Subsequently the control strategy is described, simulation results presented and conclusions and future work are discussed.

2 SYSTEM DESCRIPTION

A sketch of the burner unit is shown in Figure 1, and the functionality is explained below.

The units c, t and gg comprise the gas turbine. Fuel, $fu1$, is injected and burned in the gas generator, gg, and the hot gas leaving the combustion drives the turbine, t, which rotates the shaft of the turbocharger delivering power to drive the compression process in the compressor, c. Air is sucked in at the compressor inlet, and the hot combustion flue gas leaves the turbine to enter the second combustion chamber, the furnace, fn. Here fuel is added again, $fu2$, and another combustion takes place. More than 70% of the total fuel flow is injected into the furnace. The hot flue gas leaves the furnace and enters the boiler convection part before leaving through the funnel.

Before proceeding to the model derivation we set up some general assumptions to simplify the modelling process. These assumptions are listed and explained below.

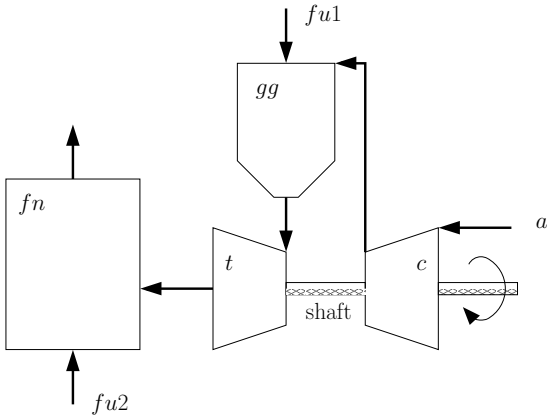

Figure 1: Drawing of the turbocharged burner system. c is the compressor, t is the turbine, gg is the gas generator (the first combustion chamber) and fn is the furnace (the second combustion chamber). a is the fresh air inlet, and $fu1$ and $fu2$ are the fuel inputs.

Assumption 2.1. *The ambient pressure is constant.*

The pressure in the engine room on a ship may vary. This will influence the pressure ratio across the compressor as inlet air is taken from the engine room. However, the setup concerned in this project is situated on shore in a test centre where ventilation is expected to cause negligible pressure variations.

Assumption 2.2. *The metal part separating the flue gas and the water-steam part consists of one piece of metal with the same temperature.*

This assumption is justified by the fact that most boilers include a pressure control loop keeping the pressure around a constant reference value, e.g. 8 bar, meaning that temperature variations are small.

Assumption 2.3. *All energy losses in the system leave through the funnel.*

This assumption is made because losses in terms of heat are negligible compared to the total amount of energy supplied to the system. A rough estimate of the relative heat losses was shown in [10] to be < 0.0002 per thousand. Furthermore, no friction losses from the shaft of the turbocharger are considered.

Assumption 2.4. *The pressure in the furnace is equal to the ambient pressure.*

Measurement performed over the convection part of the test boiler showed a pressure loss of about 9000 Pa which is small compared to the range of operation. The ambient pressure assumption is included to have consistency in the model; no fuel and air flow $\Rightarrow$ no flue gas flow.

Assumption 2.5. *The conditions in the control volumes are homogeneous.*

This assumption reflects the earlier statement that we are constructing a lumped parameter model. Furthermore, we will use a backwards place discretisation. The reason for this is that using for instance a bilinear place discretisation method introduces unwanted right half plane zeros in a linear model [11].

Assumption 2.6. *The specific heat capacity, $c_{p,f}$, and molar mass, M_f, of the flue gas throughout the process are assumed to be constant.*

An analysis of the flue gas carried out in [11] justifies this assumption. In general we do not know M_f. To find this we would have to make use of both a mass balance and a mole balance to find $M_f = \frac{m}{n}$. However, as the analysis of the flue gas in [11] shows; the molar mass of the flue gas even after as stoichiometric combustion is approximately equal to that of atmospheric air. Therefore, we assume a constant molar mass of the flue gas.

Assumption 2.7. *The flue gas can be viewed as an ideal gas.*

The reference level for the enthalpy is set to $T_0 = 273.15$ K or 0 °C, however, all temperatures are kept in kelvin (T [K]). The reason for this choice is that many of the specific heat capacity data are only available from 0 °C and up.

2.1 Modelling

The modelling is divided into two main sections: one dealing with the thermodynamic properties of the gas turbine and furnace system and another dealing with the oxygen balance. In Figure 2 the gas turbine is presented in a schematic diagram useful for modelling purposes. Attempts have been made to include the four ducts indicated on the figure in the model. This was done by using Euler equations including friction losses. However, the result of modelling these ducts did not contribute to the validity of the resulting model and will be omitted here.

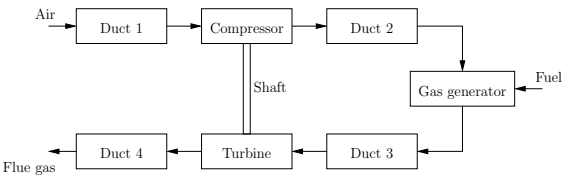

Figure 2: Schematic diagram showing the interconnection of the components that make up the gas turbine.

2.2 Turbocharger Model

There exists a lot of literature concerning mean values modelling of turbocharged engines. The results from this can be applied to this burner unit. Furthermore, the book [12] provides a good reference on turbo machinery.

Most of the modelling in this section is based on results from [3, 13, 4, 2]. As mentioned above, heat losses are neglected, and it is assumed that the processes in the compressor and turbine can be viewed as adiabatic reversible compression and expansion respectively. Such processes are called isentropic and have the following properties useful for the model derivation:

2.2.1 Properties of isentropic processes

For an ideal gas undergoing an isentropic process, the following relationship is valid [14]:

$$\left(\frac{T_{o_{is}}}{T_i}\right) = \left(\frac{p_o}{p_i}\right)^{\frac{\gamma-1}{\gamma}} \tag{1}$$

where T_i is the inlet temperature of the working fluid, $T_{o_{is}}$ is the outlet temperature under isentropic conditions. p_i and p_o are the inlet and outlet pressure respectively and the adiabatic index $\gamma = \frac{c_p}{c_v} = \frac{c_p}{c_p - \frac{R}{M_f}}$ where $R = M_f(c_p - c_v)$ also known as the ideal gas constant.

2.2.2 Compressor model

To account for the compressor not being ideal in reality, we introduce the compressor isentropic efficiency $0 \leq \eta_c \leq 1$ as the ratio between theoretical isentropic temperature rise and actual temperature rise, [14]:

$$\eta_c = \frac{T_{o_{is},c} - T_{i,c}}{T_{o,c} - T_{i,c}} \tag{2}$$

Equations (1) and (2) can be combined to find an expression for the temperature at the compressor outlet:

$$T_{o,c} = T_{i,c}\left(1 + \frac{1}{\eta_c}\left[\left(\frac{p_{o,c}}{p_{i,c}}\right)^{\frac{\gamma-1}{\gamma}} - 1\right]\right) \tag{3}$$

A common assumption when working with compressor and turbine units is to regard them as steady state steady flow processes (SSSF). The mass in the compressor and turbine is relative low compared to the mass flow rate due to the small compressor and turbine volume. Hence mass, temperature and pressure are all assumed to change instantly with changing inlet conditions rendering the dynamics negligible.

This means that the mass balance for the compressor is given as:

$$0 = \frac{dm_c}{dt} = \dot{m}_{i,c} - \dot{m}_{o,c} \tag{4}$$

Furthermore, the energy balance can be written as:

$$\begin{aligned} 0 = & \frac{d(m_c c_{p,f}(T_{o,c} - T_0) - p_c V_c)}{dt} \\ = & \dot{m}_{i,c} c_{p,f}(T_{i,c} - T_0) + \\ & - \dot{m}_{o,c} c_{p,f}(T_{o,c} - T_0) + P_c \end{aligned} \tag{5}$$

where P_c is the power delivered from the shaft to the compressor, which, using Equations (4) and (5) can be expressed as:

$$P_c = \dot{m}_c c_{p,f}(T_{o,c} - T_{i,c}) \tag{6}$$

where $\dot{m}_c = \dot{m}_{i,c} = \dot{m}_{o,c}$. Now inserting (3) into this expression gives:

$$P_c = \dot{m}_c c_{p,f} T_{i,c} \frac{1}{\eta_c} \left[\left(\frac{p_{o,c}}{p_{i,c}} \right)^{\frac{\gamma-1}{\gamma}} - 1 \right] \quad (7)$$

2.2.3 Turbine model

The turbine in the turbocharger is a fixed geometry turbine (FGT). As in case of the compressor we start by introducing the turbine isentropic efficiency $0 \leq \eta_t \leq 1$ as the ratio between actual temperature drop and theoretical isentropic temperature drop, [14]:

$$\eta_t = \frac{T_{i,t} - T_{o,t}}{T_{i,t} - T_{o_{is},t}} \quad (8)$$

Using Equations (1) and (8) an expression for the temperature at the turbine outlet can be found:

$$T_{o,t} = T_{i,t} \left(1 - \eta_t \left[1 - \left(\frac{p_{o,t}}{p_{i,t}} \right)^{\frac{\gamma-1}{\gamma}} \right] \right) \quad (9)$$

The mass and energy balances for the turbine are equivalent to those of the compressor, except that the work done by the turbine is positive so that energy is transferred from the turbine by means of work. This means that we can find an expression for the power absorbed in the shaft from the turbine:

$$P_t = \dot{m}_t c_{p,f} (T_{i,t} - T_{o,t}) \quad (10)$$

where $\dot{m}_t = \dot{m}_{i,t} = \dot{m}_{o,t}$. Inserting (9) we get:

$$P_t = \dot{m}_t c_{p,f} T_{i,t} \eta_t \left[1 - \left(\frac{p_{o,t}}{p_{i,t}} \right)^{\frac{\gamma-1}{\gamma}} \right] \quad (11)$$

2.2.4 Shaft model

The model of the shaft connecting the compressor and turbine has the purpose of describing the turbocharger speed, ω. This can be done by considering the energy balance for the shaft. The kinetic energy for the shaft is:

$$U_{kin} = \frac{1}{2} I \omega^2 \quad (12)$$

where I is the inertia of the rotating parts. Hence the energy balance is given as:

$$I\omega \frac{d\omega}{dt} = \eta_m P_t - P_c - P_f \quad (13)$$

where P_f is a friction term, which is assumed to be negligible compared to the power delivered by the turbine and the power it takes to drive the compressor. Furthermore, the mechanical efficiency, η_m, is set to 1 below. So inserting the compressor and turbine power terms from (7) and (11), the model for the shaft becomes:

$$\underbrace{\frac{1}{f_{33}}}_{} \frac{d\omega}{dt} = \underbrace{\begin{pmatrix} \dot{m}_t c_{p,f} T_{i,t} \eta_t \left[1 - \left(\frac{p_{o,t}}{p_{i,t}} \right)^{\frac{\gamma-1}{\gamma}} \right] - \\ \dot{m}_c c_{p,f} T_{i,c} \frac{1}{\eta_c} \left[\left(\frac{p_{o,c}}{p_{i,c}} \right)^{\frac{\gamma-1}{\gamma}} - 1 \right] \end{pmatrix} \Big/ (I\omega)}_{h_3} \quad (14)$$

This is the equation governing the turbocharger dynamics.

2.2.5 Turbocharger data sheets

We still need to find expressions for the flow through the compressor and turbine as well as expressions for the efficiency of these components. An overview of different methods for deriving such can be found in [3]. Some are partly based on first principle and others are functions derived from curve fitting techniques. The parameters in both approaches are estimated from turbine and compressor maps. These can be acquired from the turbocharger manufacturer.

Usually the flow and speed data are scaled to make the maps independent of the inlet conditions (p_i, T_i). The scaling is done according to:

$$\dot{\tilde{m}} = \frac{\dot{m}\sqrt{T_i}}{p_i} \left[\frac{\frac{\text{kg}}{\text{s}}\sqrt{\text{K}}}{\text{MPa}} \right], \tilde{N} = \frac{\omega}{2\pi\sqrt{T_i}} \left[\frac{1}{\text{s}\sqrt{\text{K}}} \right] \quad (15)$$

where $\tilde{N}$ is scaled rotations per second. The dependency of the speed and pressure ratios on the flow and efficiency of the compressor and turbine are:

$$\begin{bmatrix} \dot{m}_c \\ \eta_c \end{bmatrix} = g_c \left(\omega, \frac{p_{o,c}}{p_{i,c}} \right), \begin{bmatrix} \dot{m}_t \\ \eta_t \end{bmatrix} = g_t \left(\omega, \frac{p_{o,t}}{p_{i,t}} \right) \quad (16)$$

As discussed in [3], it is not always easy to find a function g_c, for the compressor map, having flow as output. An alternative mapping for the compressor is possible [3]:

$$\begin{bmatrix} \frac{p_{o,c}}{p_{i,c}} \\ \eta_c \end{bmatrix} = g_c'(\omega, \dot{m}_c) \tag{17}$$

Knowledge of the flow can be gained by introducing a control volume corresponding to the manifold connecting the compressor and the gas generator. Using the one-dimensional momentum balance for this control volume gives:

$$\frac{p_{gg} - p_{o,c}}{\rho_c} + gz\cos(\theta) + \frac{dv_c}{dt}z = -h_t(v_c) \tag{18}$$

The compressor mass flow can be found as $\dot{m}_c = \rho_c A v_c$, where A is the diameter of the pipe. This corresponds to using "Model II" in [3] . This approach has the advantages of allowing for modelling of the pressure drop over the gas generator inlet duct. However, as described in [3] the new differential equation increases model stiffness.

In this work we will use the mappings shown in (16). The data available for the turbocharger used are limited. For this reason we use a method for approximating the mappings g_c and g_t which is partly based on physical insight instead of e.g. parameterising the data by using regression to fit some polynomial model or train a neural network model. The advantage of this is that the extrapolation of data tends to give better predictions.

2.2.6 Compressor

The method used to describe the compressor flow and efficiency is described in [1]. This is the method investigated in [3] performing the best when the output is flow and efficiency. Whereas the neural network approach seems to be superior for the alternative model, in [10] the problems using a neural network model for the compressor unit under consideration was illustrated.

Expressing the enthalpy for the gas undergoing the compression as $h_{i,c} = c_{p,f}T_{i,c}$ and $h_{o,c} = c_{p,f}T_{o,c}$ for the inlet and outlet respectively, we can write Equation (6) as:

$$P_c = \dot{m}_c(h_{o,c} - h_{i,c}) = \dot{m}_c \Delta h_c \tag{19}$$

Using Equation (7) we find the following relation between the enthalpy change and the pressure ratio over the compressor:

$$\Delta h_c = c_{p,f}T_{i,c}\frac{1}{\eta_c}\left[\left(\frac{p_{o,c}}{p_{i,c}}\right)^{\frac{\gamma-1}{\gamma}} - 1\right] \tag{20}$$

Looking at the ideal case $\eta_c = 1$, $\Delta h_{c,ideal}$ can be estimated from Euler's equation for turbomachinery. For this purpose we consider a compressor with radially inclined impeller blades, no pre-whirl and no backsweep [14, p. 372-375]:

$$\Delta h_{c,ideal} = U_o C_{wo} - U_i C_{wi} \tag{21}$$

where U_o is the blade speed at the impeller tip, C_{wo}, is the tangential component of the gas velocity (whirl) leaving the impeller, U_i is the velocity of the impeller at the impeller entry and C_{wi} is the tangential component of the gas velocity entering the impeller. However, as we have assumed no pre-whirl $C_{wi} = 0$ and hence

$$\Delta h_{c,ideal} = U_o C_{wo} = U_c C_c \tag{22}$$

In practice, the whirl velocity C_c is different from the ideal $C_{c,ideal} = U_c$ due to inertia of air trapped between blades. This is known as slip, and

$$\sigma = \frac{C_c}{U_c} \tag{23}$$

is known as the slip factor. Hence:

$$\Delta h_{c,ideal} = \sigma U_c^2 \tag{24}$$

The slip factor is dependent on the mass flow rate through the compressor, meaning that the compressor pressure ratio is a function of both turbocharger speed and mass flow. The ratio between the ideal and actual enthalpy changes across the compressor is the compressor efficiency.

$$\eta_c = \frac{\Delta h_{c,ideal}}{\Delta h_c} \tag{25}$$

Using Equation (20) we have:

$$\Delta h_{c,ideal} = c_{p,f} T_{i,c} \left[\left(\frac{p_{o,c}}{p_{i,c}} \right)^{\frac{\gamma-1}{\gamma}} - 1 \right] \quad (26)$$

[1] uses these physical considerations with some empirical assumptions to derive a model for the efficiency and mass flow. They first define the dimensionless parameter Ψ, also known as the temperature coefficient or the blade loading coefficient, which is closely related to the slip factor (and the inverse square of the blade speed ratio as defined later for the turbine), as:

$$\Psi = \frac{c_{p,f} T_{i,c} \left[\left(\frac{p_{o,c}}{p_{i,c}}^{\frac{\gamma-1}{\gamma}} - 1 \right) \right]}{\frac{1}{2} U_c^2} \quad (27)$$

where $U_c = \frac{1}{2} D_c \omega$. The normalised compressor flow rate, Φ, or flow coefficient is defined as:

$$\Phi = \frac{\dot{m}_c}{\rho_a \frac{\pi}{4} D_c^2 U_c} \quad (28)$$

and the inlet Mach number M is:

$$M = \frac{U_c}{\sqrt{\gamma \frac{R}{M_f} T_{i,c}}} \quad (29)$$

The normalised flow and the compressor efficiency are assumed to be functions of Ψ and M:

$$\Phi = \frac{k_3 \Psi - k_1}{k_2 + \Psi}, \quad k_i = k_{i1} + k_{12} M \quad (30)$$

$$\eta_c = a_1 \Phi^2 + a_2 \Phi + a_3, \quad a_i = \frac{a_{i1} + a_{i2} M}{a_{i3} - M} \quad (31)$$

for $i = 1, 2, 3$. And now

$$\dot{m}_c = \Phi \rho_a \frac{\pi}{4} D_c^2 U_c \quad (32)$$

The method described in [2], based on physical insight as well, was also investigated. This method proposes a parametrisation of the enthalpy in (26) using the blade speed and the mass flow. However, the method seems not to be applicable for the compressor at hand and gives a poorer fit than the method described above.

2.2.7 Turbine

Euler's equations can also be used for the turbine, noting that by assuming no swirl at the turbine outlet the tangential component of the gas velocity at the outlet becomes zero, $C_{wt} = 0$. The rest of the equations follow the same lines as for the compressor.

However, for the turbine we use a different method for modelling flow and efficiency. Following [3] we model the flow through the turbine as the flow through nozzles (or diffusers). The well known flow equations are [12, p. 449-451]

$$\dot{m}_t = A_t \frac{p_{i,t}}{\sqrt{T_{i,t} R}} \sqrt{\frac{2\gamma}{\gamma - 1} \left[\Pi^{\frac{2}{\gamma}} - \Pi^{\frac{\gamma+1}{\gamma}} \right]} \quad (33)$$

where

$$\Pi = \max(\Pi_t, \Pi_{crit}) = \max(\frac{p_{o,t}}{p_{i,t}}, \Pi_{crit}) \quad (34)$$

Here the critical pressure ratio is: $\Pi_{crit} = \frac{2}{\gamma+1}^{\frac{\gamma}{\gamma-1}}$. A_t is the effective flow area. This is assumed to be a function of the turbocharger speed and the pressure ratio over the turbine given as:

$$A_t(\tilde{N}, \frac{p_{o,t}}{p_{i,t}}) = \quad (35)$$
$$a_2(\tilde{N}) \left(\frac{p_{o,t}}{p_{i,t}} \right)^2 + a_1(\tilde{N}) \frac{p_{o,t}}{p_{i,t}} + a_0(\tilde{N})$$

where

$$a_i(\tilde{N}) = a_{2i} \tilde{N}^2 + a_{1i} \tilde{N} + a_{0i} \quad (36)$$

this form is not standard but found to be a better fit than the suggestion in [3].

According to [3] the efficiency can be modelled as a function of the blade speed ratio:

$$\frac{U_t}{C_t} = \frac{\frac{1}{2} D_t \omega}{\sqrt{2 c_p T_{i,t} \left(1 - \left(\frac{p_{o,t}}{p_{i,t}} \right)^{\frac{\gamma-1}{\gamma}} \right)}} \quad (37)$$

where U_t is the velocity of the blade speed at the point where the flow enters, and C_t

is the tangential component of the air velocity at the entry to the turbine rotor. The efficiency is then parameterised as:

$$\eta_t = b_2(\tilde{N})\left(\frac{U_t}{C_t}\right)^2 + b_1(\tilde{N})\frac{U_t}{C_t} + b_0(\tilde{N}) \tag{38}$$

where

$$b_i(\tilde{N}) = b_{1i}\tilde{N} + b_{0i} \tag{39}$$

2.3 Gas Generator Combustion Model

In this paragraph a model used for the combustion taking place in the gas generator is described. The idea is to calculate the adiabatic flame temperature. The approach taken is to construct an artificial infinitesimal combustion control volume. The mass balance for such a control volume is given as:

$$\dot{m}_{cb,gg} = \dot{m}_c + \dot{m}_{fu1} \tag{40}$$

here $\dot{m}_c$ and $\dot{m}_{fu1}$ is the air flow and fuel supplied to the combustion, and $\dot{m}_{cb,gg}$ is the mass flow of the flue gas leaving the combustion. Likewise the energy balance is given as:

$$\dot{m}_{cb,gg}h_{cb,gg} = \dot{m}_c h_c + \dot{m}_{fu1}(h_{fu} + H_{fu}) \tag{41}$$

where h_c, h_{fu1} and $h_{cb,gg}$ are the specific enthalpies of the inflowing and outflowing fluids, and H_{fu} is the calorific value for the fuel. Rearranging to isolate $h_{cb,gg}$ gives:

$$h_{cb,gg} = \frac{\dot{m}_c h_c + \dot{m}_{fu1}(h_{fu} + H_{fu})}{\dot{m}_{cb,gg}} \tag{42}$$

Inserting $h = c_{p,f}(T - T_0)$ gives:

$$T_{cb,gg} = \begin{pmatrix} \dot{m}_c c_{p,f}(T_c - T_0) + \\ \dot{m}_{fu1}(c_{p,fu}(T_{fu} - T_0) + H_{fu}) \end{pmatrix} / (\dot{m}_{cb,gg}c_{p,f}) + T_0 \tag{43}$$

2.4 Gas Generator Model

The gas generator is treated as one control volume. The mass balance for the gas generator is given as:

$$\frac{dm_{gg}}{dt} = V_{gg}\frac{d\rho_{gg}}{dt} = \dot{m}_{i,gg} - \dot{m}_{o,gg} = \dot{m}_{cb,gg} - \dot{m}_t \tag{44}$$

where V_{gg} is the volume of the gas generator and ρ_{gg} is the density of the flue gas in the gas generator. m_{gg} is the mass of flue gas in the volume which can be expressed in terms of temperature and pressure through the ideal gas equation:

$$m_{gg} = V_{gg}\rho_{gg}, \quad \rho_{gg} = \frac{p_{gg}M_f}{RT_{gg}} \tag{45}$$

where T_{gg} is the temperature in the gas generator and p_{gg} is the pressure. The derivative of ρ_{gg} is:

$$\frac{d\rho_{gg}}{dt} = \left(\frac{M_f}{RT_{gg}}\right)\frac{dp_{gg}}{dt} - \left(\frac{p_{gg}M_f}{RT_{gg}^2}\right)\frac{dT_{gg}}{dt} = \frac{\rho_{gg}}{p_{gg}}\frac{dp_{gg}}{dt} - \frac{\rho_{gg}}{T_{gg}}\frac{dT_{gg}}{dt} \tag{46a}$$

Substituting into (44) gives:

$$\underbrace{\frac{1}{p_{gg}}}_{f_{11}}\frac{dp_{gg}}{dt} \underbrace{-\frac{1}{T_{gg}}}_{f_{12}}\frac{dT_{gg}}{dt} = \underbrace{\frac{\dot{m}_{cb,gg} - \dot{m}_t}{m_{gg}}}_{h_1} \tag{47}$$

The energy balance for the gas generator is given as:

$$\frac{d[m_{gg}c_{p,f}(T_{gg} - T_0) - p_{gg}V_{gg}]}{dt} = \dot{m}_{cb,gg}c_{p,f}(T_{cb,gg} - T_0) - \dot{m}_t c_{p,f}(T_{gg} - T_0) \tag{48}$$

Note that we have not included any energy transfer to or storage in the metal construction as these contributions are assumed to be small. Expanding the derivative gives:

$$c_{p,f}(T_{gg} - T_0)\frac{dm_{gg}}{dt} + + m_{gg}c_{p,f}\frac{dT_{gg}}{dt} - V_{gg}\frac{dp_{gg}}{dt} = \dot{m}_{cb,gg}c_{p,f}(T_{cb,gg} - T_0) - \dot{m}_t c_{p,f}(T_{gg} - T_0) \tag{49}$$

Now $\frac{dm_{gg}}{dt}$ from (44) can be substituted into (49) and by rearranging we arrive at:

$$\underbrace{-V_{gg}}_{f_{21}}\frac{dp_{gg}}{dt} + \underbrace{m_{gg}c_{p,f}}_{f_{22}}\frac{dT_{gg}}{dt} = \underbrace{\dot{m}_{cb,gg}c_{p,f}(T_{cb,gg} - T_{gg})}_{h_2} \tag{50}$$

The differential equations (14), (47) and (50) constitute the model of the gas turbine. Note that there will be a pressure drop across the gas generator which has not been included in the model.

2.5 Furnace Combustion Model

The furnace combustion model is identical to the combustion model for the gas generator described previously with a change of variables. Hence the flue gas flow and temperature from the combustion and for the furnace can be written as:

$$\dot{m}_{cb,fn} = \dot{m}_t + \dot{m}_{fu2} \tag{51}$$

and

$$T_{cb,fn} = \begin{pmatrix} \dot{m}_t c_{p,f}(T_t - T_0) + \\ \dot{m}_{fu2}(c_{p,fu}(T_{fu} - T_0) + H_{fu}) \end{pmatrix} / (\dot{m}_{cb,fn} c_{p,f}) + T_0 \tag{52}$$

respectively.

2.6 Furnace Model

The furnace model is supposed to capture the temperature dynamics in the furnace. Such a model might be divided into multiple control volumes including the convection tubes to achieve a more accurate model. However, here we focus one a single control volume. The mass balance is:

$$\frac{dm_{fn}}{dt} = \dot{m}_{cb,fn} - \dot{m}_{fn} \tag{53}$$

Where $\dot{m}_{fn}$ is the flue gas flow leaving through the funnel. As the pressure in the furnace is regarded as constant, $p_{fn} = p_a$, the energy balance becomes:

$$\frac{[dm_{fn} c_{p,f}(T_{fn} - T_0)]}{dt} = -\dot{Q} + \dot{m}_{cb,fn} c_{p,f}(T_{cb,fn} - T_0) - \dot{m}_{fn} c_{p,f}(T_{fn} - T_0) \tag{54}$$

where T_{fn} is the furnace temperature and $\dot{Q} = \alpha_{c,fn}(T_{fn} - T_m)$ is the energy transferred to the metal wall of the furnace and convection part with T_m being the temperature of the wall and $\alpha_{c,fn}$ being the heat transfer coefficient. Expanding the derivatives using (53) and rearranging gives:

$$\underbrace{\frac{1}{f_{44}}}\frac{dT_{fn}}{dt} = \underbrace{\frac{\dot{m}_{cb,fn} c_{p,f}(T_{cb,fn} - T_{fn}) - \dot{Q}}{m_{fn} c_{p,f}}}_{h_4} \tag{55}$$

where m_{fn} is found from:

$$m_{fn} = \rho_{fn} V_{fn} = \frac{p_{fn} M_f}{R T_{fn}} V_{fn} \tag{56}$$

where V_{fn} is the volume of the furnace.

Before finding the output mass flow, $\dot{m}_{fn}$, the change in density, ρ_{fn}, of the flue gas must be found. Such derivations are equivalent to those in (46) and as the pressure is constant, the first term in (46a) is zero leaving the following equation for the change in density:

$$\frac{d\rho_{fn}}{dt} = -\frac{\rho_{fn}}{T_{fn}} \frac{dT_{fn}}{dt} \tag{57}$$

which together with (53) and (55) gives the mass flow:

$$\dot{m}_{fn} = \frac{\dot{m}_{cb,fn} c_{p,f}(T_{cb,fn} + T_0) - \dot{Q}}{(T_{fn} + T_0) c_{p,f}} \tag{58}$$

2.7 Oxygen Model

The oxygen model is divided into two; one describing the oxygen fraction, x_{gg,O_2}, in the gas generator and another describing the oxygen fraction, x_{fn,O_2}, in the furnace. These models do not treat the combustion meaning that the inputs to these models are the outputs from the combustion. However, the two models are very similar and will be treated in general. First we put up the mole balance for the control volume:

$$\frac{dn}{dt} = \dot{n}_i - \dot{n}_o \tag{59}$$

where $\dot{n}_i$ and $\dot{n}_o$ are the mole flows entering and leaving the container respectively and n is the number of moles accumulated. Now the mole balance for the oxygen can be expressed as:

$$\frac{d(n x_{o,O_2})}{dt} = \dot{n}_i x_{i,O_2} - \dot{n}_o x_{o,O_2} \tag{60}$$

using a backward difference place discretisation, differentiating gives:

$$n\frac{dx_{o,O_2}}{dt} + x_{o,O_2}\frac{dn}{dt} = \dot{n}_i x_{i,O_2} - \dot{n}_o x_{o,O_2} \tag{61}$$

Substituting (59) into this expression and rearranging gives:

$$\frac{dx_{o,O_2}}{dt} = \frac{1}{\tau}(x_{i,O_2} - x_{o,O_2}) \qquad (62)$$

where, the time constant is $\tau = \frac{n}{\dot{n}_i}$. Remember also that we can find n as $n = \frac{pV}{RT} = \frac{m}{M_f}$. Using the fact that M_f for the flue gas is assumed constant gives the time constant as $\tau = \frac{m}{\dot{m}_i}$. For the gas generator and furnace the equations are:

$$\underbrace{1}_{f_{55}} \frac{dx_{gg,O_2}}{dt} = \underbrace{\frac{1}{\tau_{gg}}(x_{cb1,O_2} - x_{gg,O_2})}_{h_5} \qquad (63)$$

and

$$\underbrace{1}_{f_{66}} \frac{dx_{fn,O_2}}{dt} = \underbrace{\frac{1}{\tau_{fn}}(x_{cb2,O_2} - x_{fn,O_2})}_{h_6} \qquad (64)$$

respectively.

As is apparent from these equations we need to know both, n_i and x_{i,O_2} to make use of the differential equation. These are determined by studying the combustion taking place.

2.7.1 Combustion in gas generator

The combustion is assumed to be complete. A complete combustion is a process which burns all the carbon C to CO_2, all the hydrogen H to H_2O and all sulfur S to SO_2. If there are any unburned components in the exhaust gas such as C, H_2 and CO the combustion process is incomplete. The mole flows of carbon and hydrogen coming in with the fuel are:

$$\dot{n}_{C1} = \frac{\dot{m}_{fu1} y_C}{M_C}, \quad \dot{n}_{H1} = \frac{\dot{m}_{fu1} y_H}{M_H} \qquad (65)$$

where y_C and y_H are the mass fractions of carbon and hydrogen in the fuel. We assume here that $y_H = 1 - y_C$ hence ignoring sulphur and other purely represented components in diesel and heavy fuel used for marine boilers.

We assume that the atmospheric air for the combustion consists of 21% O_2 and 79% N_2, here the percentages represent mole percentage and we denote the oxygen fraction as $x_{O_2,atm}$. Next the reaction schemes for the process are laid down to be able to determine how much oxygen is left in the flue gas after combustion and what the different compounds in the flue gas are. Reaction schemes:

$$\dot{n}_C \mathrm{C} + \dot{n}_C \mathrm{O_2} \longrightarrow \dot{n}_C \mathrm{CO_2} \qquad (66)$$

$$\dot{n}_H \mathrm{H} + \frac{1}{4}\dot{n}_H \mathrm{O_2} \longrightarrow \frac{1}{2}\dot{n}_H \mathrm{H_2O} \qquad (67)$$

Hence the mole flow of oxygen leaving the combustion is:

$$\dot{n}_{cb1,O_2} = \dot{n}_{c,O_2} - (\dot{n}_{C1} + \frac{1}{4}\dot{n}_{H1}) \qquad (68)$$

where $\dot{n}_{c,O_2} = \dot{n}_c x_{O_2,atm}$ with $\dot{n}_c = \frac{\dot{m}_c}{M_{air}} = \frac{\dot{m}_c}{M_f}$. We also have $\dot{n}_{N_2,c} = \dot{n}_c(1 - x_{O_2,atm})$. Finally, the total amount of moles leaving the combustion is given as:

$$\dot{n}_{cb1} = \dot{n}_{cb,O_2} + \dot{n}_{N_2} + \dot{n}_C + \frac{1}{2}\dot{n}_H \qquad (69)$$

This equation works only for combustion with atmospheric air as is the case in the gas generator. The reason is that we do not keep track of the components in the flue gas during the rest of the process. However, we notice that, as we have assumed that M_f is constant, we can find the total amount of mole leaving the combustion as $\dot{n}_{cb1} = \frac{\dot{m}_c + \dot{m}_{fu1}}{M_f}$. The expression for the oxygen fraction entering the gas generator then becomes:

$$x_{cb1,O_2} = \frac{\dot{n}_{cb1,O_2}}{\dot{n}_{cb1}} = \frac{\dot{m}_{cb1,O_2}}{\dot{m}_{cb1}} \left(\frac{M_f}{M_{O_2}}\right) \qquad (70)$$

Now in the mean time the last bracket on the right hand side of Equation (70) is close to unity ($M_f/M_{O_2} \approx 0.9$). Hence an approximate solution could be obtained by treating the mole and mass fraction as equal.

2.7.2 Combustion in furnace

The derivation of the expression for the oxygen fraction of the flue gas leaving the furnace combustion is identical to that of the gas generator combustion due to the assumption of constant molar mass of the

flue gas. The combustion air is the flue gas leaving the turbine having the oxygen fraction x_{gg,O_2}. The oxygen fraction is given as:

$$x_{cb2,O_2} = \frac{\dot{n}_{cb2,O_2}}{\dot{n}_{cb2}} \tag{71}$$

2.7.3 Fuel

In relation to combustion we need to know what fuel we are using to find out the ratio between carbon and hydrogen. In case of heavy fuel, one can order an analysis of the fuel to obtain such data. In case of diesel we assume that we know the structure of the main molecule. Assuming that it consists only of carbon and hydrogen atoms the general molecule looks like:

$$\text{Diesel}: \quad \mathrm{C}_X\mathrm{H}_Y \tag{72}$$

The mole fraction of carbon and hydrogen in the diesel can be found as:

$$x_C = \frac{X}{X+Y}, \quad x_H = 1 - x_C = \frac{Y}{X+Y} \tag{73}$$

From this we can find the average molar mass of diesel as:

$$\bar{M}_{fu} = x_C M_C + x_H M_H \tag{74}$$

and so the mass fractions of carbon and hydrogen are:

$$y_C = x_C \frac{M_C}{\bar{M}_{fu}}, \quad y_H = x_H \frac{M_H}{\bar{M}_{fu}} \tag{75}$$

In this work we assume $X = 15$ and $H = 32$.

2.8 Model Summary

The total model is best presented in descriptor form as:

$$F(x)\frac{dx}{dt} = h(x,u,d) \tag{76a}$$

$$y = g(x,u,d) \tag{76b}$$

where $x = [p_{gg}, T_{gg}, \omega, T_{fn}, x_{gg,O_2}, x_{fn,O_2}]^T$, $u = [\dot{m}_{fu1}, \dot{m}_{fu2}]^T$, $d = [T_a, T_{fu}, T_m]^T$, and $y = [\dot{m}_{fu}, \dot{Q}, x_{fn,O_2}]^T$, $\dot{m}_{fu} = \dot{m}_{fu1} + \dot{m}_{fu2}$. Expanding, (76a) has the form:

$$\begin{bmatrix} f_{11} & f_{12} & 0 & 0 & 0 & 0 \\ f_{21} & f_{22} & 0 & 0 & 0 & 0 \\ 0 & 0 & f_{33} & 0 & 0 & 0 \\ 0 & 0 & 0 & f_{44} & 0 & 0 \\ 0 & 0 & 0 & 0 & f_{55} & 0 \\ 0 & 0 & 0 & 0 & 0 & f_{66} \end{bmatrix} \begin{bmatrix} \frac{dp_{gg}}{dt} \\ \frac{dT_{gg}}{dt} \\ \frac{d\omega}{dt} \\ \frac{dT_{fn}}{dt} \\ \frac{dx_{gg,O_2}}{dt} \\ \frac{dx_{fn,O_2}}{dt} \end{bmatrix} = \begin{bmatrix} h_1 \\ h_2 \\ h_3 \\ h_4 \\ h_5 \\ h_6 \end{bmatrix} \tag{77}$$

where the elements f_{ij} and h_i were indicated in the model derivation in Equations (14), (47), (50), (55), (63) and (64).

F is never singular, hence it has a well defined inverse, so (76a) can be written as an ordinary differential equation: $\dot{x} = f(x,u,d) = F^{-1}(x)h(x,u,d)$.

2.9 Model Verification

Preliminary test data have been collected from AI's test centre. These are used to verify the constructed model. In Figure 3 both the measurement data and the simulation outputs are shown.

It should be mentioned that the measurement of the temperature at the turbine inlet is unreliable as the sensor was placed close to the gas generator outlet where sufficient gas mixing had not yet occurred, meaning that the temperature was very dependent on the placement in the cross section. Instead the turbine outlet temperature is shown in the plot. However, this measurement has a large time constant not modelled. Also the actual gas generator pressure is not measured, and the data shown are constructed from another measurement of differential pressure across the turbine, assuming close to ambient pressure at the turbine outlet. Finally, the measurement of the fuel input is based on the return pressure in the fuel line to each burner rather than the mass flow measurement.

For these reasons the parameters in the model are estimated on the basis of the shaft velocity and oxygen level alone and a low weighted funnel temperature. The parameters that were estimated using quadratic prediction error performance criteria were: fuel calorific value H_{fu}, heat transfer coefficient $\alpha_{c,fn}$, inertia of turbocharger shaft I.

The figure shows good agreement between model and measurement data in terms of capturing the dynamical behaviour, however, in terms of stationary values these are not represented well by the model for other outputs than the oxygen level. The pressure, temperature and shaft speed differences can be due to poor turbocharger maps, however, it can also originate from the non-modelled pressure

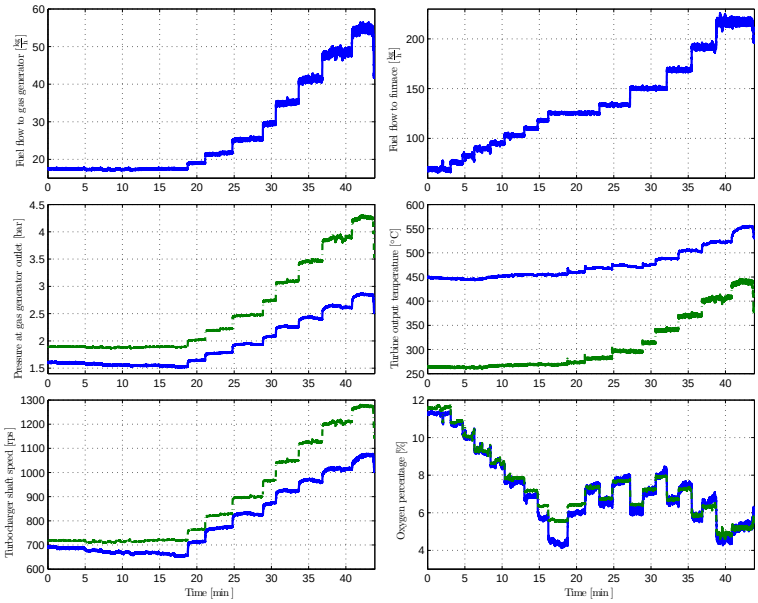

Figure 3: Comparison between measurements (blue solid curves) and simulation output (green dashed curves).

losses over the gas generator or the pipes leading from and to the compressor and turbine, which can be introduced by allowing at least one more control volume, and by using Bernoulli's equations. Attempts to model pipe losses have, however, not improved the model. For now we accept these discrepancies as our purpose is to develop an oxygen controller.

2.10 Control Properties

In this section some control properties of the system are discussed. It is obvious that the burner can be operated in two modes; one where only the gas turbine is running and one where both the gas turbine and furnace burner are on. The first mode is less interesting and below we will only address the second. The focus is on the feasible steady state fuel input distribution, optimal steady state fuel distribution and nonlinearities in the dynamics and gain.

The control objectives are to follow the fuel flow setpoint or in fact a power setpoint while optimising efficiency and keeping a clean combustion, measured as an oxygen level above 3 %.

In Figure 4 the steady state oxygen level in the flue gas leaving the funnel is shown as a function of the two fuel flows. The plot indicates the feasible steady state fuel flows as the input region where the oxygen level is above 3 %. Note that this region is convex.

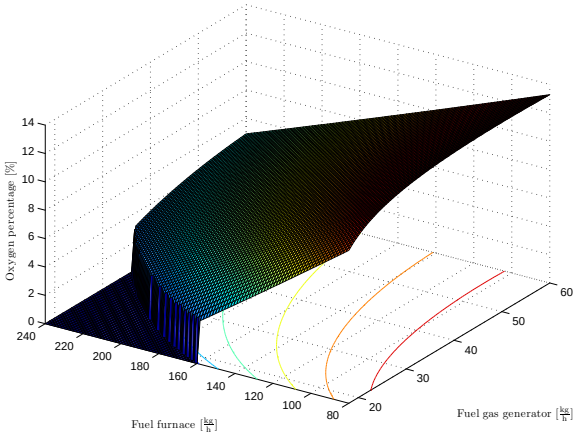

Figure 4: Flue gas oxygen percentage as a function of the two fuel flows. The region where the oxygen percentage is ≥ 3 % is indicated in the figure. Note that this region is convex.

Further, in Figure 5 a plot of the power delivered to the furnace walls as a function of the total fuel input is shown. From this plot it can be seen that at all times the fuel flow to the gas generator should be kept at a minimum, respecting the oxygen constraint, to achieve the highest efficiency of

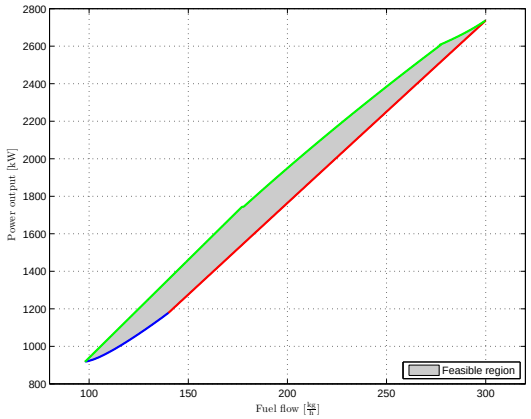

Figure 5: Plot of the burner power output as a function of the total fuel flow supply. For any fuel flow between minimum and maximum there are infinitely many ways to distribute the two fuel flows. As can be seen only one choice is optimal. The blue curve corresponds to increasing the gas generator fuel alone. The red curve corresponds to increasing only the furnace fuel flow. The green curve is the optimal amount of fuel for a given load. Finally, the grey area is the feasible region.

the burner.

If needed for control design or model estimation, the curve of optimal fuel distribution can be determined on line using simple experiments.

To illustrate the nonlinear behaviour of the system, normalised step responses of linear models linearised along the optimal fuel input distribution from minimum to maximum load are shown in Figure 6. The normalisation is done with respect to the absolute value of the local model steady state gain. From these plots it is obvious that the dynamics change remarkably over the burner operating range. Further, it is noticed that the response from $\dot{m}_{fu1}$ to the oxygen level included a non-minimum phase behaviour. This can limit the performance if a loop is closed around this subsystem. However, it turns out that the inverse response is not pronounced, meaning that the undershoot is relatively small and even difficult to spot in measurements, though it does introduce a delay of < 1 s. It is worth noting that these local linear models of 6th order are well approximated

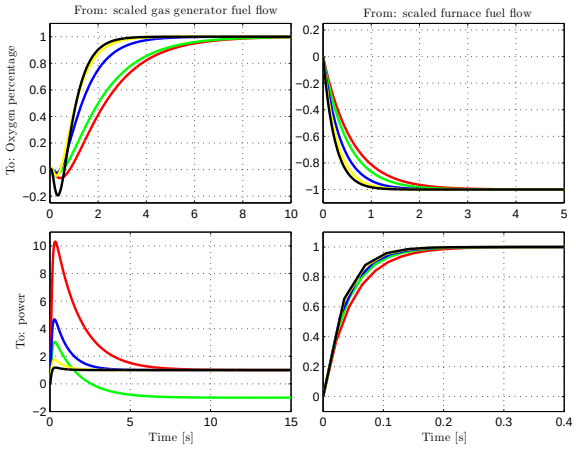

Figure 6: Normalised step responses from fuel flows to the oxygen level in the funnel and power delivered to the metal. The responses are made from linear models gathered from linearising the model over the load range with optimal fuel distribution. The colour ordering is as follows with the first colour being the lowest load: red, green, blue, yellow and black.

by 3rd order models using Hankel norm model reduction – see e.g. [15].

In Table 1 the static gains used in the normalisation before are shown as a function of the static fuel flow. This table shows that not only the dynamics but also the gain in the system change remarkably over the operating range.

These properties might be necessary to incorporate in a controller design which will be discussed in the following section. In control of turbocharged diesel engines one of the concerns is the temperature of the inlet air to the turbine and outlet of the compressor as too high temperatures can accelerate wear and cause breakdowns.

Table 1: Steady state gains from fuel input to oxygen level and power output for changing burner load along the optimal fuel distribution curve.

Load $[\frac{\text{kg}}{\text{h}}]$	98.00	180.71	228.05	275.39	290.00
$\frac{x^{ss}_{fn,O_2}}{\dot{m}^{ss}_{fu1}}$	17.99	34.29	14.90	7.02	2.75
$\frac{x^{ss}_{fn,O_2}}{\dot{m}^{ss}_{fu2}}$	-15.90	-15.02	-11.90	-9.84	-8.58
$\frac{\dot{Q}^{ss}}{\dot{m}^{ss}_{fu1}}$	1.50	-4.95	2.87	7.20	10.72
$\frac{\dot{Q}^{ss}}{\dot{m}^{ss}_{fu2}}$	73.58	73.25	71.66	70.11	68.85

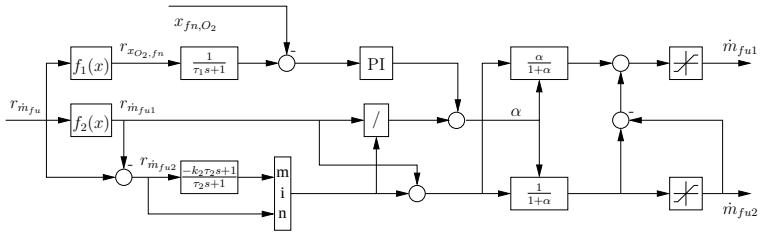

Figure 7: Control structure for the burner unit. A nonlinear feedforward is combined with some dynamic compensation to take into account the dynamics of the process. A feedback around the oxygen is closed to handle disturbances and model uncertainty.

However, in the present setup there are no control authority to adjust this temperature independently of the gas generator inlet fuel. Further, there does not seem to be problems with too high temperatures during load changes, caused by the dynamics of the gas generator, which could have limited the gradient at which the load could be increased or decreased. For these reasons constraints on these temperatures are not included in the controller design but could be converted into constraints on the input. This means that the mechanical design of the gas turbine should be such that too high temperatures are never achieved at the turbine inlet and compressor outlet. If such temperatures are detected during operation, it could be due to a mechanical fault, and the unit should be stopped for service or a different control strategy should be inserted to limit the gas turbine load till service has been carried out. It could also be due to disturbances or changing environment/operating conditions and in these cases a control strategy taking these external factors into account could be used or the input constraints could be adjusted. However, in this preliminary work we do not focus on this special situation.

3 CONTROLLER DESIGN

There exist many approaches to fuel/air control of which a few were mentioned in the book on PID controllers, [6]. One of the approaches was based on selector control and another on ratio control. The advantages of selector control is the way to avoid lack of air flow when increasing burner load. However, these approaches are based on the measurement and control of air flow, whereas in the present setup only fuel flow and oxygen level are measured, and the air flow is not directly controlled. We propose a variant of ratio control presented in Figure 7.

Note that this controller consists of a feedback and a feedforward path. The feedforward from the total fuel flow reference, $r_{\dot{m}_{fu}}$ is functions calculating optimal steady state values for the fuel distribution, $r_{\dot{m}_{fu1}} = f_2(r_{\dot{m}_{fu}})$, $r_{\dot{m}_{fu2}} = r_{\dot{m}_{fu}} - r_{\dot{m}_{fu1}}$, and the corresponding oxygen level, $r_{x_{fn,O_2}} = f_1(r_{\dot{m}_{fu}})$. Note that no compensation is made for disturbances. The feedforward functions are calculated by inverting the steady state version of the model presented in this paper. The functions can be approximated by piecewise quadratic functions consisting of three pieces. The dynamic lag filter, $\frac{k_2\tau_2 s+1}{\tau_2 s+1}$, introduced after the nonlinear feedforward function for $r_{\dot{m}_{fu2}}$ is introduced to accommodate the non-minimum phase behaviour to x_{fn,O_2} when changing $\dot{m}_{fu1}$. The "min" block ensures that air lack never occurs. The other filter, $\frac{1}{\tau_1 s+1}$, has a time constant close to that of the closed loop oxygen response. The feedback, a PI controller, adjusts the ratio, $\alpha = \frac{\dot{m}_{fu1}}{\dot{m}_{fu2}}$, between the two fuel flows to correct the oxygen level if the feedforward compensation is not accurate due to disturbances or model uncertainty. Note that the reference for the oxygen level might also be incorrect. Antiwindup compensation, not shown, is made for the PI controller. The input saturation configuration to the right in the diagram ensures that the reference can be achieved even though $\dot{m}_{fu2}$ has saturated.

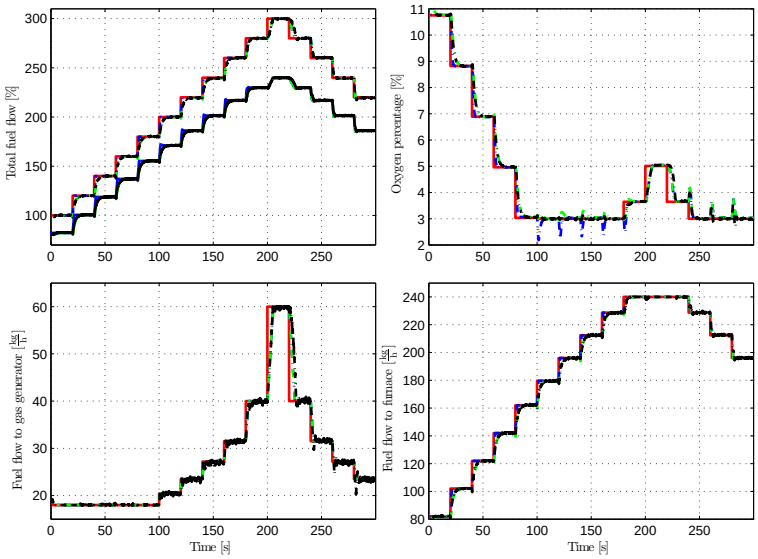

Figure 8: Simulation results with a staircase reference change to the total fuel flow. The total fuel flow is shown in the top left plot, upper curves, along with the power delivered to the metal divided by the fuel enthalpy, lower curves. The oxygen percentage is shown in the top right plot. The fuel flow to the gas generator is shown in the bottom left plot and the fuel flow to the furnace in the bottom right plot. The red lines in the top plots are reference curves. The red lines in the bottom plots are feedforward signals. The blue curves are the uncontrolled system with pure feedforward. The green curves have feedforward and the lag filter in the feedforward path. The black curves have both feedforward and feedback.

4 SIMULATION RESULTS

In this section we show some simulation result, applying the controller presented in the previous section to the nonlinear model of the burner unit. We show two simulations. The first illustrates the ability of the controller to track the reference. The second shows the ability to suppress disturbances (which to some degree can also be seen as model uncertainty). All simulation plots contain four curves. One curve shows the effect of the nonlinear feedforward (blue), the second the effect of the lag filter (green), the third the effect of the feedback (black) and the fourth is the reference values and feedforward signals (red). The plot showing total fuel flow contains seven curves. The lower ones correspond to the power delivered to the metal in the boiler divided by the specific enthalpy of the fuel, $h_{fu} = c_{p,fu}(T_{fu} - T_0) + H_{fu}$.

In Figure 8 the setpoint for the fuel flow/power output from the burner is ramped up and down.

Note that the feedback and the dynamic term in the feedforward have slowed the response down. However, a more accurate oxygen control is achieved. The burner unit control will normally be in an inner cascade configuration with an outer boiler pressure controller, and even though the response has been slowed down it is still considerably faster than can be expected of the response of any boiler pressure loop.

In Figure 9 changes in input disturbances, compressor inlet air pressure and temperature corresponding to changing conditions in the engine room are made.

Note that both the pressure and temperature disturbances have a large impact on the burner process. Especially a much higher fuel flow for the gas generator is needed to keep a clean combustion when both inlet air pressure drops and the temperature rises. This might in the worst case limit the maximum possible power from the burner. As these disturbances have not been included in the steady state

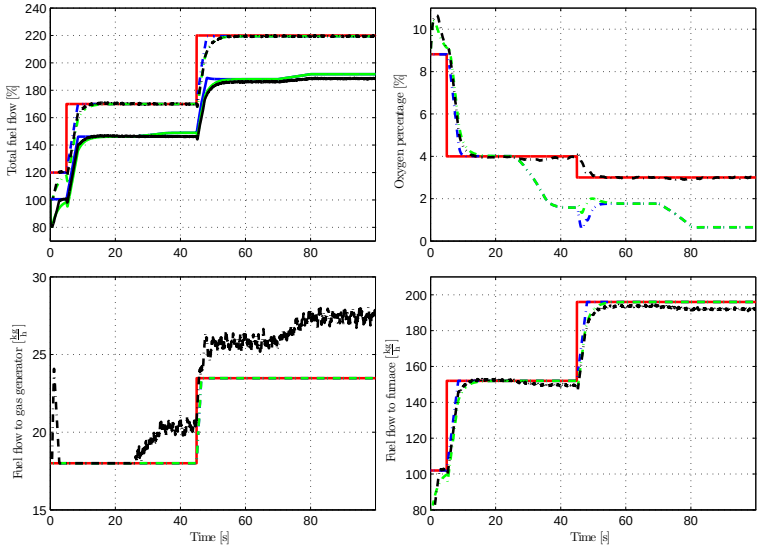

Figure 9: Simulation results with a ramp disturbance in engine room pressure of $-500\ \frac{\text{Pa}}{\text{s}}$ over 10 s, from 25 s to 35 s. Further, a ramp disturbance occurs in the engine room temperature of $3\ \frac{^\circ\text{C}}{\text{s}}$ over 10 s from 70 s to 80 s. The total fuel flow is shown in the top left plot; upper curves, along with the power delivered to the metal divided by the fuel enthalpy; lower curves. The oxygen percentage is shown in the top right plot. The fuel flow to the gas generator is shown in the bottom left plot and the fuel flow to the furnace in the bottom right plot. The red lines in the top plots are reference curves. The red lines in the bottom plots are feedforward signals. The blue curves are the uncontrolled system with pure feedforward. The green curves have feedforward and lag filter in the feedforward path. The black curves have both feedforward and feedback.

feedforward calculations the effect will be the same as model uncertainty. This indicates that robustness can be achieved with a rather simple controller. However, as the controller adjusts oxygen to a predetermined reference curve, the performance cannot be optimal in case of disturbances and uncertainty as the current oxygen reference curve does not match the operating conditions.

5 CONCLUSION

In this paper we have developed a model of a turbocharged burner unit for boiler applications. This model is based on first principles. Dynamically the model performs well, however, the static gains have offsets and increase with load. Further, measurements are required to determine the source of the discrepancies.

The control properties of the derived model were discussed, and both the dynamics and gains of the model proved to be highly nonlinear. Further, it was noted that there is an optimal distribution between the gas generator and furnace fuel flows.

Though nonlinear, a simple controller proved to be able to control the burner in the presence of reference changes and disturbances. This controller was based on a nonlinear feedforward from the calculated optimal fuel distribution accompanied by a feedback on oxygen to ensure a clean combustion.

It is argued that when uncertainties and disturbances are present, optimal performance cannot be achieved. A more sophisticated control strategy is needed in these cases to approximate optimality.

5.1 Future Work

Further, measurements from the plant are needed to find the reason for the differences between model and plant data. Also, further analysis is needed to study the sensitivity of the burner performance to disturbance changes as inlet pressure

and temperature. Also, does the plant dynamics and gains change remarkably as the disturbance changes?

A simple nonlinear model for the gas generator can be derived by neglecting variations in mass and internal energy – see [5].

A control strategy that is particularly suited for this type of control problem is MPC. The reason for this is that MPC naturally handles the constraints present on input and process variables. Further, a model of the disturbances can easily be introduced and optimal performance can be approximated. However, application of linear MPC shows poor performance possibly due to the nonlinearities in the plant. This means that one could consider nonlinear MPC or linear MPC with multiple models or perhaps simple multiple nonlinear models. It should here be noted that the feasible input region was found to be convex.

REFERENCES

[1] J. P. Jensen, A. F. Kristensen, S. C. Sorenson, N. Houbak, E. Hendricks, Mean value modelling of a small turbocharged diesel engine, SAE Technical Paper Series No. 910070.

[2] M. Müller, E. Hendricks, S. C. Sorenson, Mean valve modelling of turbocharged spark ignition engines, SAE Technical Paper Series 980784 (1998) 125–145.

[3] I. Kolmanovsky, P. Moraal, Turbocharger modeling for automotive control applications, SAE Technical Paper Series 1999-01-0908.

[4] M. Jung, K. Glover, Control-oriented linear parameter-varying modelling of a turbocharged diesel engine, in: Proceedings of the IEEE Conference on Control Applications, 2003.

[5] R. Sekhon, H. Bassily, J. Wagner, J. Gaddis, Stationary gas turbines – a real time dynamic model with experimental validation, in: American Control Conference, Minneapolis, Minnesota, USA, 2006.

[6] K. J. Åström, T. Hägglund, Advanced PID Control, ISA - Instrumentation, Systems, and Automation Society, 2006.

[7] J. M. Maciejowski, Predictive Control With Constraints, Harlow: Pearson Education Limited, 2001.

[8] J. A. Rossiter, Model-based Predictive Control: A Practical Approach, CRC Press LLC, 2003.

[9] S. J. Qin, T. A. Badgwell, A survey of industrial model predictive control technology, Control Engineering Practice 11 (2003) 733–764.

[10] R. B. Persson, B. V. Sørensen, Hybrid control of a compact marine boiler system, Master's thesis, Aalborg University, Institute of Electronic Systems (2006).

[11] P. U. Hvistendahl, B. Solberg, Modelling and multi variable control of a marine boiler, Master's thesis, Aalborg Universitet, Institute of Electronic Systems, Aalborg, Denmark (2004).

[12] H. I. H. Saravanamuttoo, G. F. C. Rogers, H. Cohen, Gas Turbine Theory, 5th Edition, Prentice Hall, 2001.

[13] A. Amstutz, L. Guzzella, Control of diesel engines, IEEE Control Systems Magazine 18 (5) (1998) 53–71.

[14] T. D. Eastop, A. McConkey, Applied Thermodynamics for Engineering Technologists, Addison Wesley Longman, 1993.

[15] K. Zhou, J. Doyle, K. Glover, Robust and Optimal Control, New Jersey: Prentice-Hall, Inc, 1996.